

New insights about HERG blockade obtained from protein modeling, potential energy mapping, and docking studies

Ramy Farid,^{a,*} Tyler Day,^a Richard A. Friesner^b and Robert A. Pearlstein^a

^a*Schrödinger, Inc., 120 West Forty-Fifth Street, 32nd Floor, New York, NY 10036, USA*

^b*Department of Chemistry, Columbia University, New York, NY 10036, USA*

Received 11 October 2005; revised 15 December 2005; accepted 16 December 2005

Available online 18 January 2006

Abstract—We created a homology model of the homo-tetrameric pore domain of HERG using the crystal structure of the bacterial potassium channel, KvAP, as a template. We docked a set of known blockers with well-characterized effects on channel function into the lumen of the pore between the selectivity filter and extracellular entrance using a novel docking and refinement procedure incorporating Glide and Prime. Key aromatic groups of the blockers are predicted to form multiple simultaneous ring stacking and hydrophobic interactions among the eight aromatic residues lining the pore. Furthermore, each blocker can achieve these interactions via multiple docking configurations. To further interpret the docking results, we mapped hydrophobic and hydrophilic potentials within the lumen of each refined docked complex. Hydrophilic iso-potential contours define a ‘propeller-shaped’ volume at the selectivity filter entrance. Hydrophobic contours define a hollow ‘crown-shaped’ volume located above the ‘propeller’, whose hydrophobic ‘rim’ extends along the pore axis between Tyr652 and Phe656. Blockers adopt conformations/binding orientations that closely mimic the shapes and properties of these contours. Blocker basic groups are localized in the hydrophilic ‘propeller’, forming electrostatic interactions with Ser624 rather than a generally accepted π -cation interaction with Tyr652. Terfenadine, cisapride, sertindole, ibutilide, and clofilium adopt similar docked poses, in which their N-substituents bridge radially across the hollow interior of the ‘crown’ (analogous to the hub and spokes of a wheel), and project aromatic/hydrophobic portions into the hydrophobic ‘rim’. MK-499 docks with its longitudinal axis parallel to the axis of the pore and ‘crown’, and its hydrophobic groups buried within the hydrophobic ‘rim’.

© 2005 Elsevier Ltd. All rights reserved.

1. Introduction

The human ether-a-go-go related gene (HERG) potassium channel is a key cardiac ion channel that regulates the duration of the plateau phase of the cardiac action potential.^{1–3} Delayed activation of HERG due to chemical blockade, or certain types of inherited dysfunction, results in increased duration of ventricular repolarization, appearing as a prolongation of the time interval between the Q and T waves (LQT) in the electrocardiogram. LQT is considered a major risk factor for torsades de pointes, a life-threatening arrhythmia.⁴ Diverse types of organic compounds are believed to disrupt HERG current upon binding within the lumen of the homo-tetrameric pore domain.⁵ Since the discovery of the connection

between HERG blockade and LQT, several drugs subsequently identified as potent LQT causing HERG blockers have been withdrawn from the market. Potencies of such blockers, measured via patch-clamp electrophysiology, range from low nM (e.g., sertindole) to more than 50 μ M (e.g., grepafloxacin). HERG activity is now routinely monitored during all stages of pre-clinical lead optimization to ensure that safe levels are met prior to clinical development. Potent HERG blockade or LQT induction effects represent obvious safety concerns. Lower potency blockade may likewise be of concern when HERG versus primary target IC₅₀, or HERG IC₅₀ versus therapeutic plasma concentration, fall outside of the required safety margins.⁶

Much effort has been directed over the last several years toward understanding the chemical requirements for HERG blockade. Such knowledge could be used to identify and triage potential HERG blockers present in chemical collections and mitigate activity present in HERG-afflicted series during lead optimization.⁷ Molec-

Keywords: HERG potassium channel; HERG blockers; Homology modeling; Induced fit; Terfenadine; MK-499; Cisapride; Sertindole; Clofilium; Ibutilide.

* Corresponding author. Tel.: +1 646 366 9555; fax: +1 646 366 9550; e-mail: ramy@schrodinger.com

ular modeling has been used extensively to search for properties that promote blockade and for interpreting site-directed mutagenesis data. In particular, several ligand-based quantitative structure–activity relationship (QSAR) and pharmacophore models built using structurally diverse compounds have been published over the last few years.^{8–14} A set of key pharmacophore features, consisting of two or more hydrophobic/aromatic groups surrounding a central basic group, are predicted by most ligand-based models. A CoMSiA-based 3D QSAR modeling study performed by Pearlstein et al. predicted a set of pharmacophore features falling loosely within two major substructures (referred to as ‘head’ and ‘tail’ regions).⁸ The head region contains one aromatic group, an optional second aromatic or hydrophobic group, and an optional basic center located 6–8 Å from the requisite aromatic group, which enhances activity when present. The CoMSiA model is least certain in the tail region, which exhibits greater chemical variability and conformational flexibility than the head. The CoMSiA data set (Table 1) consists of several diverse blockers, including sertindole, an anti-psychotic drug withdrawn due to LQT effects (HERG IC_{50} = 3 nM), and analogs of sertindole with systematic modification and deletion of functional groups aimed at isolating the critical pharmacophore features. Remarkably, high levels of activity were retained by the sertindole analogs despite large chemical modifications, including deletion of the tail region.⁸ This may underlie the known difficulties in mitigating HERG activity (especially when a large decrease in potency is required).

HERG-blocker binding interactions can only be indirectly inferred, given the absence of co-crystal structures. Key binding-sensitive residues in the S6 helix have been determined from ala-scanning mutagenesis for a small, but growing, list of known blockers.^{5,15–17} Such studies have demonstrated that all potent blockers are highly sensitive to Tyr652Ala and Phe656Ala mutation. The occurrence of Tyr and Phe at both of these sequence positions is unique to HERG and EAG potassium channels, whereas blockade sensitive spatial positions of these side chains appear to be unique to HERG.^{4,17} Sensitivity to Ala mutations at additional blocker-specific sequence positions has also been demonstrated, for example, Val625Ala and Gly648Ala specifically affect MK-499, clofilium, and ibutilide.^{5,15} Mapping the spatial positions of Tyr652, Phe656, and other residues within the protein, and predicting the nature of ligand interactions and bound conformations via docking, could lead to improvements in the prediction and mitigation of HERG activity. Such knowledge could also help explain the susceptibility of HERG (an unintentional binding site) to chemical blockade, a phenomenon that has not been observed with other human potassium channels.

We created a homology model of the homo-tetrameric pore domain of HERG based on the crystal structure of the bacterial potassium channel KvAP. We opened and closed the pore relative to its original size in KvAP, and mapped the positional variation of blockade sensitive residues determined from site-directed mutagenesis.

We used our model to dock eleven published HERG blockers, including a subset of sertindole analogs from the CoMSiA data set.⁸

2. Computational methods

2.1. Protein structure modeling

The structures of the S5 (outer), pore, and S6 (inner) helices of HERG and other potassium channels are believed to be homologous to those of the three structurally known bacterial potassium channels KcsA, MthK, and KvAP, as suggested from multiple sequence alignments.²⁵ We used Prime 1.1 (Schrödinger, LLC, Portland, OR) to align the HERG S5, pore (P), and S6 sub-sequences to those of the KvAP monomer (1orq) obtained from the RCSB Protein Data Bank (Fig. 1). Major differences in the sequences of the pore domain of HERG compared to the bacterial channels include the S5-P segment (a structurally complex 22-residue insertion in HERG between residues 583 and 604^{18,19}), and the presence of both Tyr and Phe at positions 652 and 656, respectively, in the S6 helix of HERG. The S5-P insertion, which is remote from the putative binding site, was omitted from the alignment (and therefore not built) due to its absence in the KvAP template. A homology model of the tetrameric pore domain was built from the aligned sub-sequences by first using Prime to build the monomer and then using the refinement module in Prime (PLOP, Protein Local Optimization Program^{20–23}) to predict the conformation of the interfacial side chains in the context of the entire 4-fold symmetric structure. Steric complementarity of the inter-monomer interfaces and preservation of 4-fold symmetry were achieved using this approach. The symmetry operators describing the relative orientation of the four monomers were obtained from the crystallographic information included in the 1orq PDB file.

The degree of pore opening varies in the three bacterial crystal structures, ranging from closed in KcsA to open in KvAP, to somewhat more open in MthK. The observed differences in pore opening between KcsA and MthK may represent inherent differences in the gating properties of the three channels or different snapshots along a common gating trajectory. The latter interpretation was proposed due to the high degree of superimposability of the selectivity filter regions upstream from the Gly hinge in the S6 helix.²⁴ The relationship between the degree of pore opening in HERG and the structural properties of the ion conduction cavity relative to blocker binding is currently unknown. We explored the effects of pore opening on the shape, side-chain positions, and properties of the ion conduction cavity, as well as docking results. The backbone ϕ and ψ torsion angles of residues near the known hinge positions S6:Gly648 and S5:Gly572 of each monomer of the tetrameric HERG homology model were modified manually in unison (thus maintaining 4-fold symmetry) to effect further opening or closing of the pore. The fully closed and open HERG models compared well with KcsA and

Table 1. HERG blockers studied using 'induced fit' docking^{8,15}

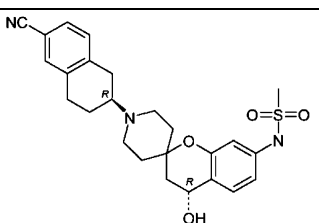
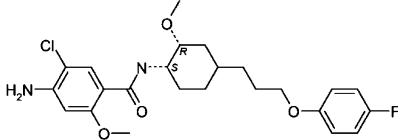
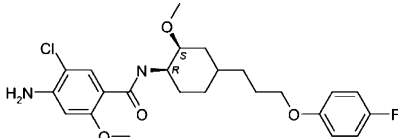
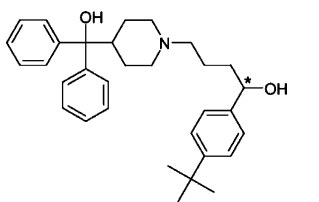
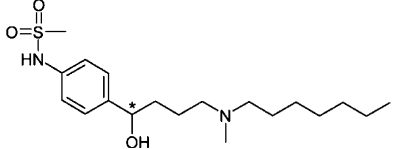
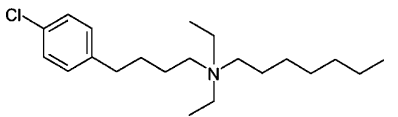
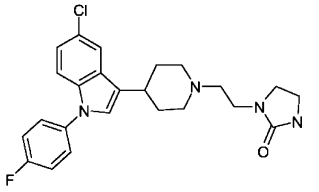
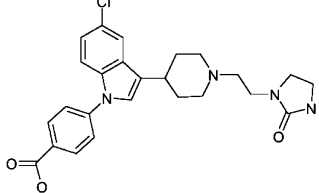
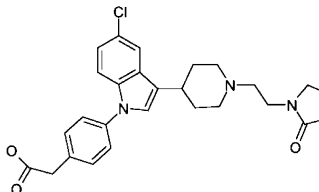
Blocker	Structure	IC ₅₀ (nM)
MK-499		34
(-)-Cisapride		45
(+)-Cisapride		45
(RS)-Terfenadine		56
(RS)-Ibutilide		28
Clofilium		ND
Sertindole		3
Sertindole A1		75,000
Sertindole A2		579

Table 1. (continued)

Blocker	Structure	IC ₅₀ (nM)
Sertindole A3		36
Sertindole A4		131
Sertindole A5		11

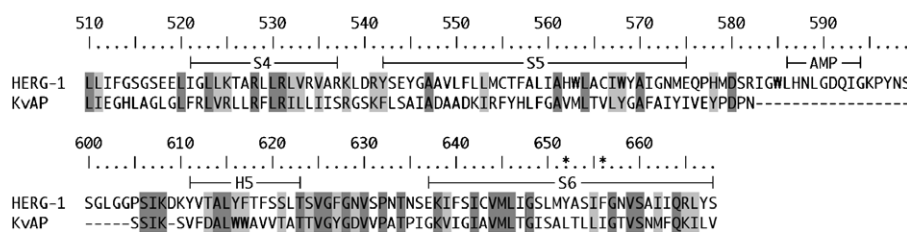


Figure 1. Sequence alignment between HERG and KvAP. Phe652 and Tyr656 are indicated with an asterisk in the ruler.

MthK, respectively, based on graphical inspection of the superimposed structures (not shown).

2.2. Docking

Docking studies of the following compounds were performed using Glide 3.0 (Schrödinger, LLC, Portland, OR), followed by side-chain searching and minimization in Prime ('induced fit docking' protocol): *R*- and *S*-enantiomers of terfenadine, α -[4-(1,1-dimethylethyl)phenyl]-4-(hydroxydiphenylmethyl)-1-piperidinebutanol; the two diastereomers of cisapride, (\pm)-*cis*-4-amino-5-chloro-*N*-[1[3-((4-fluorophenoxy)-propyl)]-3-methoxy-4-piperidiny]-2-methoxybenzamide²⁵; MK-499, (+)-*N*-[1'-(6-cyano-1,2,3,4-tetrahydro-2(*R*)-naphthalenyl)-3,4-dihydro-4(*R*)-hydroxyspiro(2*H*-1-benzopyran-2,4'-piperidin)-6-yl]methanesulfonamide monohydrochloride; clofilium, 4-chloro-*N,N*-diethyl-*N*-heptylbenzenebutanaminium; *R*- and *S*-enantiomers of ibutilide, *N*-[4-[4-(ethylheptylamino)-1-hydroxybutyl]phenyl]methanesulfonamide; sertindole, 1-[2-[4-[5-chloro-1-(4-fluorophenyl)-1*H*-indol-3-yl]-4-piperidiny]ethyl]-2-imidazolidinone; and five sertindole analogs (A1–A5 in Table 1). All of these compounds were selected for docking based on their known structure–activity relationships: ligand-based for the sertindole series; protein-based (via mutagenesis) for terfenadine, cisapride, MK-499, clofilium,

and ibutilide. The docking and scoring algorithms of Glide have been fully described elsewhere.^{26,27} The induced fit protocol, also described elsewhere,²⁸ is intended to circumvent the inflexible binding site requirement of grid-based docking through use of post-docking refinement steps. Briefly, each blocker was docked into the ion conduction cavity of the open form of the HERG homology model using the standard precision (SP) scoring mode of Glide. van der Waals radii of the ligand and protein were scaled down by 50% to compensate for the lack of protein flexibility during docking, and 20 poses were generated for each ligand in order to sample a wide range of possible docking modes. In situ refinement of the predicted protein–ligand complexes was then performed using Prime. First, all side chains within a 5.0 Å radius of each docked ligand pose were searched using Prime's side-chain sampling algorithms. This was followed by energy minimization of each docked protein–ligand complex (complete residues within a 5.0 Å radius of each docked ligand pose) using the OPLS2001 force-field and Prime's implicit solvent model. The ligands were then re-docked into their corresponding receptor structures using Extra Precision (XP) scoring in Glide. The resulting docked poses were superimposed by rigid body rotation of the complexes about the 4-fold symmetry axis to facilitate visual comparison. The top scoring docked poses of each blocker

(based on GlideScore and Prime energy) were analyzed and compared. In cases where several poses were identified with nearly identical GlideScores and Prime energies, the pose that showed greatest consistency with available mutagenesis data was selected for further analysis. Hydrophobic/ring stacking interactions were qualitatively flagged based on contact between the molecular surfaces of individual side chains and docked ligands. Although an attempt was made to distinguish between hydrophobic versus ring stacking effects, and also between sandwich, parallel displaced, and T-shaped π - π interactions, no attempt was made to quantify the energetic contribution of each of these interactions to the overall binding energy.

Polar interactions were flagged based on the presence of hydrogen bonds or close proximity of ionic groups. Interactions were also evaluated using hydrophobic and hydrophilic iso-potential energy contour maps calculated with Sitemap (Schrödinger, LLC, Portland, OR). Default hydrophobic and hydrophilic contour levels (-0.5 and -6.0 , respectively) were used for all calculations. Occupation of predicted hydrophobic and hydrophilic volumes by docked ligand substructures was used to help understand the basis for the predicted binding modes.

All computations were carried out on a Linux (RedHat 7.3) cluster with 1.6 GHz AMD64 Opteron processors.

3. Results

3.1. Protein modeling

The spatial positions of Tyr652 and Phe656 side chains are predicted from our homology model to face the interior of the conduction pathway (Fig. 2), in agreement with other published HERG homology models.^{5,8,15,29} This, together with the dependence of blockade on wild type (or similar) residues at these sequence positions,

suggests their direct involvement in binding interactions.^{5,15–17} Our results further suggest that the spatial positions of Tyr652 and Phe656 side chains are highly sensitive to variation in backbone conformation of S6:Gly648 and S5:Gly572, becoming compressed into a smaller volume toward the intracellular base of the selectivity filter in the maximally closed (Fig. 3A) versus maximally open (Fig. 3B) models. Thus, channel opening both exposes the ligand binding pocket, and promotes a highly effective concentration of aromatic side chains within that pocket. The following key structural features of the open pore domain are predicted from our homology model:

1. Intra-monomer side-chain packing is predicted between Thr623, Ser624, and Val625 side chains. Thr623 and Tyr625 side chains are packed together via methyl and aromatic groups, respectively (Fig. 4).
2. Tyr652 and Phe656 side chains are approximately one turn apart and face toward the central axis of the pore. The Tyr side chains are more orthogonal to the pore axis than those of Phe, possibly due to packing constraints with Thr623 (Fig. 2).
3. Val625, Thr623, Ser624, Tyr652, Phe656, and Val659 are packed along the inter-monomer interface (Fig. 3B).

Hydrophobic and hydrophilic potentials were mapped within the intracellular pore region of the homology model prior to induced fit docking (Fig. 5). The three-dimensional hydrophobic contours consist of a continuous, 'crown-shaped' volume that stems largely from the eight aromatic side chains. Additionally, four large 'prong-like' elements project from the crown's rim toward the intracellular direction, and four smaller prongs project between the selectivity filter and S6 helix (these elements enlarge through induced fit docking of some blockers). The crown-shaped hydrophobic volume ranges from 10.3 to 12.0 Å in diameter (measured relative to the intracellular facing 'prongs', which comprise the lowest energy region of the contours). Additionally, a

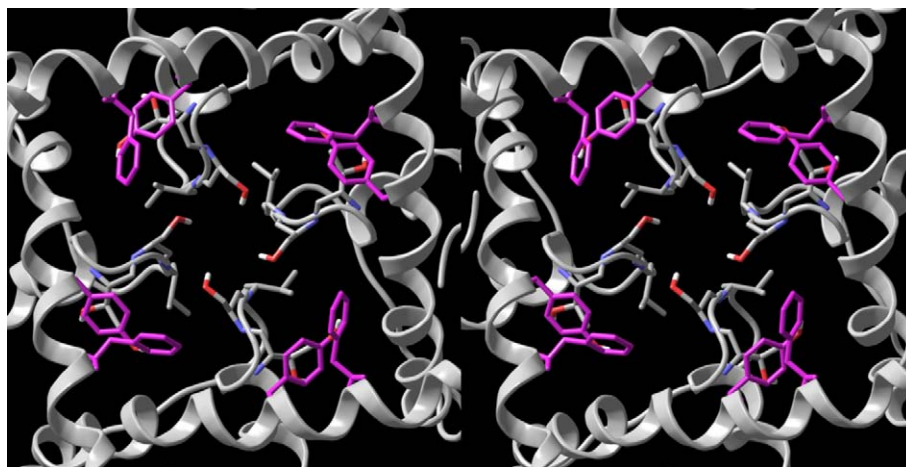


Figure 2. Stereo ribbon drawing of the homology model (open form) used in the docking studies. The structure is viewed parallel to the central pore axis, looking from the intracellular end toward the selectivity filter. Thr623, Ser624, Val625, Tyr652, and Phe656 are shown in stick representation. Tyr652 and Phe656 are shown in magenta, Ser624 and Val625 are in the center of the figure, and Thr623 is partially obscured by Tyr652 and Phe656.

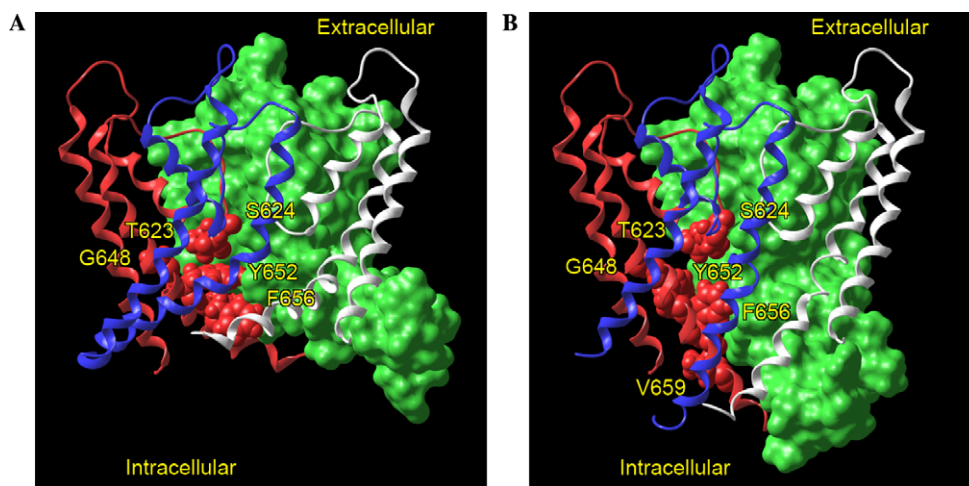


Figure 3. (A) Closed form of the homology model, showing the four monomers in different colors. Molecular surfaces of key binding sensitive residues identified from mutagenesis studies are drawn for one monomer (color-coded red). The side chains of all of these residues, except for Gly648, are predicted to pack against the adjacent monomer (color-coded green). (B) Open form of the homology model. The positions of Phe656, Tyr652, and Val659 (not visible) are shifted toward the selectivity filter relative to the closed form, and Tyr652 has rotated toward the central axis of the pore. Re-packing of the side chains of these residues relative to the closed form is predicted.

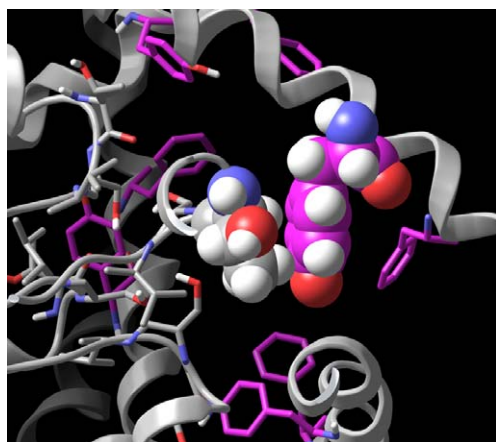


Figure 4. Open form of the homology model highlighting (in one of the monomers) the predicted close packing between the side chains of Thr623 and Tyr652 (magenta).

small, star-shaped hydrophobic volume is predicted at the base of the selectivity filter, centered on the pore's central axis. A large 'propeller-shaped' hydrophilic volume is predicted between the intracellular base of the selectivity filter and the extracellular facing prongs of the hydrophobic crown-shaped region. The hydrophilic propeller stems largely from the four polar side chains of Ser624 and backbone nitrogen and oxygen atoms in this region. We measured distances between the lowest energy reference points in the hydrophobic (i.e., intracellular facing prongs) and hydrophilic iso-potential energy volumes. These distances range from 5.6 to 7.8 Å, depending on the choice of reference points. This separation is consistent with the 6–8 Å distance between the basic center and required aromatic group in the 3D QSAR model of Pearlstein et al.⁸ The hydrophilic and hydrophobic volumes undergo considerable changes in the docked complexes in response to ligand-

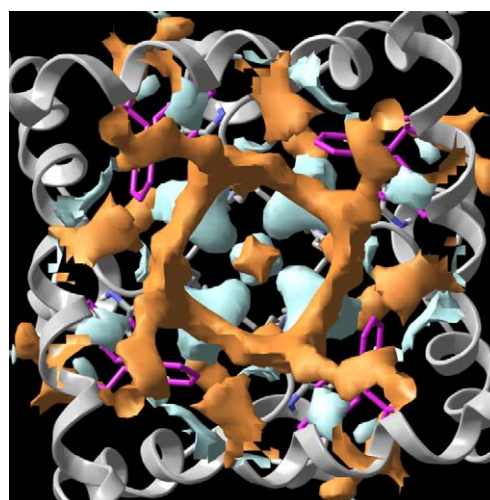


Figure 5. Hydrophilic (cyan) and hydrophobic (orange) iso-potential energy contours calculated within the potassium conduction pathway of the homology model prior to induced fit docking (same view as in Fig. 1). A crown-shaped hydrophobic volume surrounds the central axis of the pore. A propeller-shaped hydrophilic volume is sandwiched between the intracellular base of the selectivity filter and the bottom aspect of the crown-shaped hydrophobic volume. A small, star-shaped hydrophobic volume is located at the hub of the propeller-shaped hydrophilic volume.

induced protein conformational changes that occur during the post-docking refinement steps. This results in optimal spatial matching between the physicochemical properties of the protein and each blocker.

3.2. Induced fit docking

The compounds listed in Table 1 were docked into an opened form of the homology model (relative to the original KvAP structure) using the induced fit protocol described in the computational methods section. Both

enantiomers of the racemic blockers ibutilide and terfenadine were docked, as were the two known diastereomers of cisapride.²⁵ and the single known diastereomer of MK-499. In the case of ibutilide, terfenadine, and cisapride, the different stereoisomers for each compound were found to adopt very similar poses and conformations. Although stereospecific HERG blockade has been attributed to bupivacaine.³⁰ and verapamil,³¹ stereospecific blockade by ibutilide, terfenadine, or cisapride has not been reported, consistent with our results.

Multiple simultaneous aromatic ring stacking and/or hydrophobic interactions are predicted between Tyr652 and Phe656 side chains and aromatic/hydrophobic blocker groups in the docking poses. Furthermore, such interactions are apparent in multiple docking poses of each blocker. Table 2 summarizes these interactions and also highlights the number of qualitatively estimated sandwich, parallel displaced, T-shaped (edge-to-face),

Table 2. Summary of aromatic ring stacking and hydrophobic interactions between side chains of Tyr652 and Phe656 and the blockers

Blocker	Number of aromatic residues in contact with blocker	
	Tyr652	Phe656
MK-499	2	2 (t)
(–)-Cisapride	4 (t)	1 (pd)
(+)-Cisapride	3 (2t)	2 (pd)
<i>S</i> -Terfenadine	4 (2t)	2 (t,pd)
<i>R</i> -Terfenadine	4 (2t)	2 (2t)
<i>R</i> -Ibutilide	3	1
<i>S</i> -Ibutilide	3 (t)	1
Clofilium	3 (t)	4 (2t)
Sertindole	3 (t,e)	1
Sertindole A1	2 (t)	1 (pd)
Sertindole A2	2 (t)	1 (pd)
Sertindole A3	2 (t)	1 (pd)
Sertindole A4	1	2 (s,e)
Sertindole A5	2 (t)	1 (t)

Nature of π – π interactions is shown in parentheses: t, T-shaped; pd, parallel displaced; s, sandwich; e, edge-to-edge.

and edge-to-edge π – π interactions. Quantum chemical calculations^{32–34} indicate that both stacked and T-shaped aromatic structures constitute stable minima in the gas phase and likely contribute additional stabilization beyond the free energy gain resulting from burial of hydrophobic groups. Additional studies reveal that various substituents on the aromatic groups affect interaction energies³⁵ and others suggest that aromatic/aliphatic and aromatic/aromatic T-shaped interactions have degenerate energies.^{36,37} We made no attempt in this study to quantify the energetic contribution of ring stacking interactions to binding, as the resolution of the induced fit models is likely not sufficiently high to justify such calculations.

Tyr652 was proposed in several previous studies to undergo π -cation interactions with the basic group present in most blockers.^{8,9,12,16} However, spatial proximity between basic groups and Tyr652 is not observed in the docked poses of any blocker included in our study. Therefore, π -cation interactions are not predicted from our docking results. However, the extensive ring stacking and hydrophobic interactions predicted from our docking studies with Tyr652 and Phe656 are consistent with the published mutagenesis studies.^{8,15,5}

What follows is a detailed analysis of the induced fit models for each of the blockers in Table 1.

3.3. Terfenadine

Six aromatic side chains (four Tyr652 and two Phe656 residues) are predicted to simultaneously interact with *S*-terfenadine (Fig. 6A). Four of these six aromatic interactions involve T-shaped π – π stacking. The pose for *R*-terfenadine (not shown) is nearly identical to that of *S*-terfenadine. The only significant difference is that one of the T-shaped interactions with *S*-terfenadine is replaced by a parallel displaced interaction with *R*-terfenadine. These results are consistent with mutagenesis studies. Additionally, three and four hydrogen bonds are predicted for *S*- and *R*-terfenadine, respectively. For *S*-terfenadine, these are to the backbone oxygen

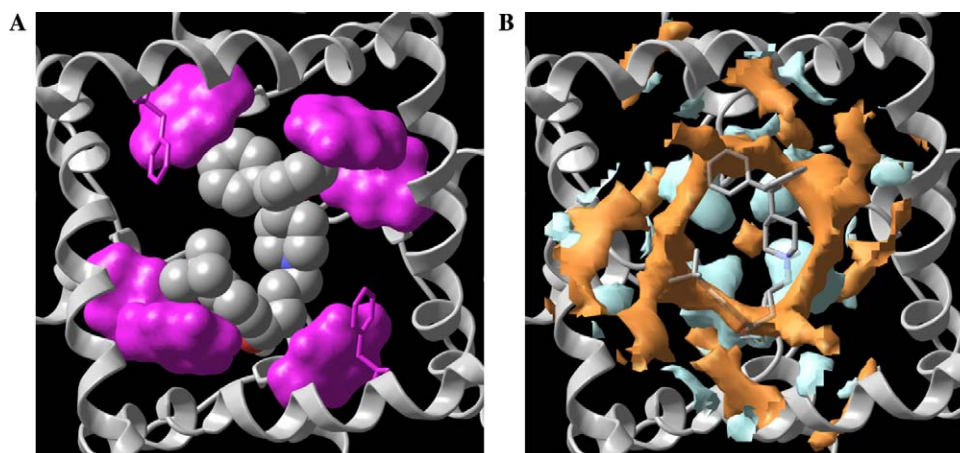


Figure 6. (A) Induced fit docking pose showing molecular surface contacts of the side chains of Tyr652 and Phe656 (magenta) with *S*-terfenadine. (B) Overlap of *S*-terfenadine with the hydrophobic (orange) and hydrophilic (cyan) iso-potential energy contours. Hydrogen atoms are not shown.

of Leu622 and side chains of Ser649 and Ser624. For *R*-terfenadine, three of the hydrogen bonds occur with different Ser624 side chains and the fourth is to the side chain of Tyr652. However, the importance of the predicted hydrogen bonds cannot be validated from the available mutagenesis data. The three aromatic rings, *t*-butyl group, and butyl chain of both terfenadine enantiomers partially occupy the crown-shaped hydrophobic volume (Fig. 6B). The two hydroxyl groups in terfenadine partially occupy the propeller-shaped hydrophilic volume at the intracellular base of the selectivity filter. The piperidine ring nitrogen (basic center) also occupies this hydrophilic volume.

3.4. Cisapride

Simultaneous interactions are predicted between (+)-cisapride and five aromatic side chains, three to Tyr652 and two to Phe656 (Fig. 7A). T-shaped π - π stacking interactions are observed between (+)-cisapride and two Tyr652 side chains on opposite sides of the channel. A parallel displaced interaction with one

Phe656 side chain is also observed. Additionally, hydrogen bonds are predicted between Ser624 and amide NH, and an adjacent Ser624 and piperidine NH of (+)-cisapride. The sensitivity of cisapride to Ser624Ala mutation was not determined and therefore the latter interactions cannot be validated. The pose for (–)-cisapride (not shown) is very similar to that of (+)-cisapride. There is one less interaction with a Phe656, but that is replaced by an additional interaction with a Tyr652 residue. The two aromatic rings of both diastereomers of cisapride partially occupy the crown-shaped hydrophobic volume (Fig. 7B). A methylene group of the piperidine ring occupies the star-shaped hydrophobic volume. The amide and piperidine basic groups of cisapride partially occupy the propeller-shaped hydrophilic volume.

3.5. MK-499

Simultaneous interactions are predicted between the more rigid MK499 and four aromatic side chains; two each with Tyr652 and Phe656, including T-shaped π - π stacking with one of the latter side chains

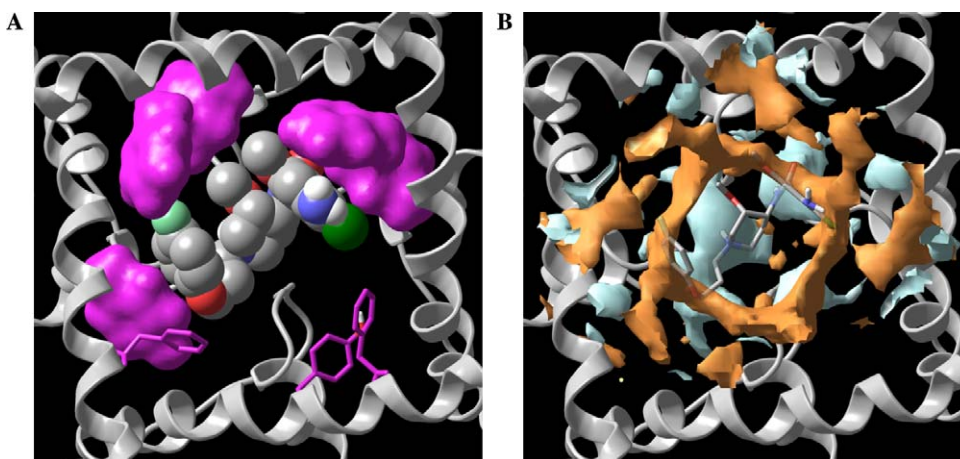


Figure 7. (A) Induced fit docking pose showing molecular surface contacts of the side chains of Tyr652 and Phe656 (magenta) with (+)-cisapride. (B) Overlap of (+)-cisapride with the hydrophobic (orange) and hydrophilic (cyan) iso-potential energy contours. Hydrogen atoms are not shown.

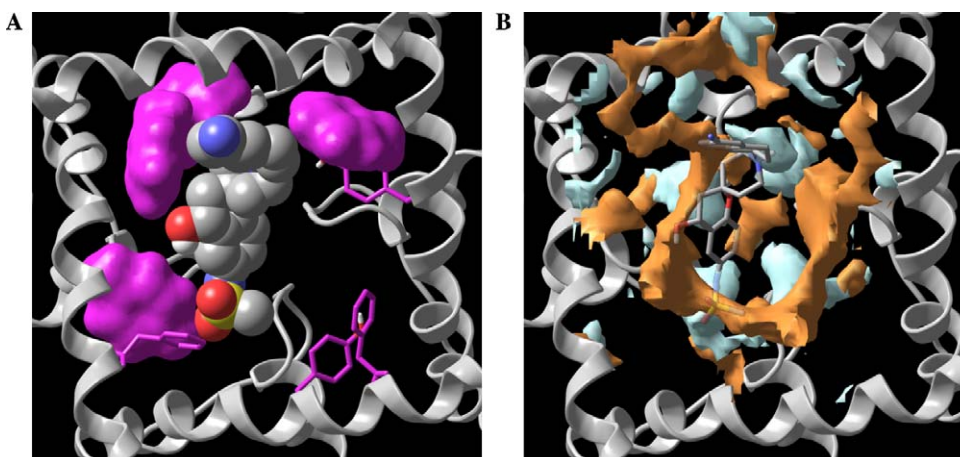


Figure 8. (A) Induced fit docking pose showing molecular surface contacts of the side chains of Tyr652 and Phe656 (magenta) with MK499. (B) Overlap of MK499 with the hydrophobic (orange) and hydrophilic (cyan) iso-potential energy contours. Hydrogen atoms are not shown.

(Fig. 8A). Additionally, the following residues are within interaction distance to MK-499: Ser624 (4), Ser649 (3), Thr623 (1), and Ala653 (1); numbers in parentheses indicate the number of monomers interacting with MK-499. Also, the side chain of one Val625 residue is within 5 Å of MK-499. The binding sensitivity of MK-499 to mutation of Thr623, Ser624, and Val625 residues has been demonstrated.⁵ Direct interaction between MK-499 and Gly648 is not predicted, despite the demonstrated sensitivity of binding to Gly648Ala. The sensitivity of MK-499 to this mutation appears to represent indirect effects on cavity size, that is, pore opening, or shape associated with alterations in conformational properties of this key hinge residue. Several examples in which mutation of residues not directly in contact with the ligand result in dramatic effects on binding and/or activity have been reported in the literature.^{38,39} MK-499 may be more sensitive than other blockers to changes in gating properties associated with mutation of this S6 hinge residue due to its location in the pore, which is predicted to be different from the other blockers that we studied. The hydrophobic and hydrophilic volumes present in the HERG/MK-499 complex differ substantially from those of terfenadine and cisapride (Fig. 8B). The crown-shaped hydrophobic volume present for the other blockers is highly disrupted due to side-chain conformational differences associated with the induced fit refinement of MK-499. One region of this volume is partially occupied by the cyano-tetrahydronaphthyl moiety of MK-499. Another region is partially occupied by the phenyl and methyl groups of the phenylmethanesulfonanilide moiety. The NH and oxygens of the methanesulfonanilide group occupy the propeller-shaped hydrophilic volume. As for other blockers, the basic piperidine nitrogen of MK-499 also occupies the propeller-shaped volume. MK-499 docks with its long principal axis parallel to the central axis of the pore, projecting its methanesulfonanilide into a ‘prong’ of the hydrophobic ‘crown’ between the S6 helix and selectivity filter. This binding mode (similar to that predicted by Pearlstein et al.⁸) differs from other blockers we studied, consistent with mutagenesis results.⁵

3.6. Ibutilide

Simultaneous interactions are predicted between the aliphatic groups of *S*-ibutilide and four aromatic side chains; three with Tyr652 and one with Phe656 (Fig. 9A). One of the interactions with Tyr652 is T-shaped π - π stacking. Additionally, hydrogen bonds are predicted between the methanesulfonanilide NH of ibutilide and Ser624, and between the NH of the basic center and adjacent Ser624 (assuming binding of the protonated form). *R*-Ibutilide makes similar interactions, but its pose is a mirror image of that of *S*-ibutilide. The mirror plan is parallel to the pore axis and lies between adjacent S6 helices. The crown-shaped hydrophobic volume is partially occupied by the septane chain (especially the last four methylene groups) and the aromatic group (Fig. 9B). The basic center of ibutilide occupies the propeller-shaped hydrophilic volume located at the base of the selectivity filter. These results are consistent with mutagenesis studies.¹⁵

3.7. Clofilium

Simultaneous interactions are predicted between clofilium and seven aromatic side chains, including all four Tyr652 residues and three Phe656 residues (Fig. 10A). The chlorophenyl group is involved in three T-shaped π - π stacking interactions with one Tyr652 and two Phe656 side chains. The chlorophenyl group, septyl chain, and ethyl chains of clofilium occupy a large fraction of the crown-shaped hydrophobic volume in the docked complex (Fig. 10B). The propeller-shaped hydrophilic volume is partially occupied by the quaternary nitrogen. Long washout times were observed for clofilium relative to ibutilide in wild type HERG. Perry and co-workers attributed this effect to a direct interaction between the chlorophenyl group of clofilium and Ser624.¹⁵ Increased washout times were not observed for clofilium in the Ser624Ala mutant. The sensitivity of clofilium washout time to Ser624Ala may be explained by stronger electrostatic interactions between the permanently charged group of clofilium and the propeller-shaped hydrophilic region (largely contributed by

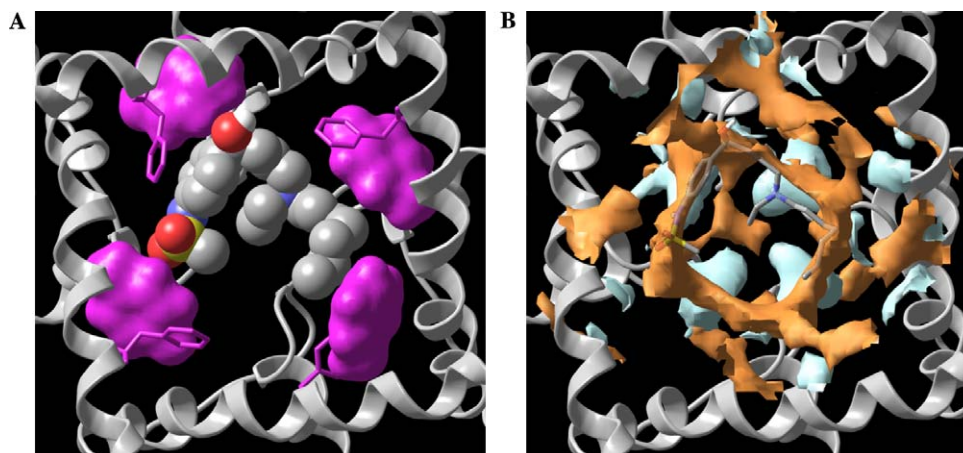


Figure 9. (A) Induced fit docking pose showing molecular surface contacts of the side chains of Tyr652 and Phe656 (magenta) with *S*-ibutilide. (B) Overlap of *S*-ibutilide with the hydrophobic (orange) and hydrophilic (cyan) iso-potential energy contours. Hydrogen atoms are not shown.

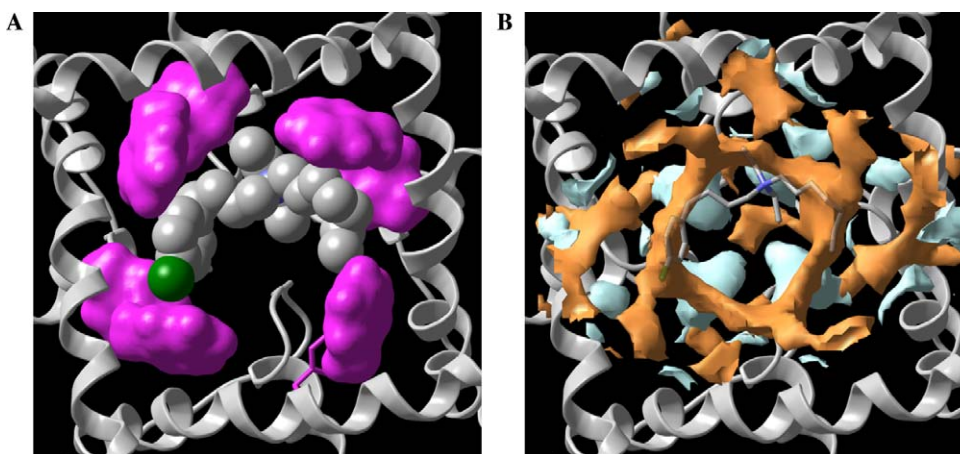


Figure 10. (A) Induced fit docking pose showing molecular surface contacts of the side chains of Tyr652 and Phe656 (magenta) with clofilium. (B) Overlap of clofilium with the hydrophobic (orange) and hydrophilic (cyan) iso-potential energy contours. Hydrogen atoms are not shown.

Ser624) compared to those of the tertiary nitrogen of ibutilide. This is consistent with the proximity of the basic groups of clofilium and ibutilide to the hydrophilic region predicted from our docking results for these compounds.

3.8. Sertindole

Simultaneous interactions are predicted between sertindole and four aromatic side chains, including three Tyr652 residues and one Phe656 residue (Fig. 11A). A T-shaped π - π stacking interaction occurs with the side chain of Tyr652. Binding sensitivity to mutation of Tyr652 and Phe656 has not been studied for sertindole. Therefore, we cannot rule out the possibility of alternate binding modes for sertindole or its analogs compared to terfenadine, cisapride, and other blockers with known sensitivity to these mutations. The crown-shaped hydrophobic volume is partially occupied by the fluoro-phenylindole moiety and two methylene groups of the piperidine ring (Fig. 11B). The imidazolidinone group

also partially occupies this volume. The imidazolidinone NH occupies the propeller-shaped hydrophilic volume.

3.9. Sertindole A5

Sertindole A5 forms simultaneous interactions with two Tyr652 side chains and one Phe656 (Fig. 12A). Two T-shaped π - π stacking interactions are observed, one to Tyr652 and the other to Phe656. Additionally, the backbone oxygen of Thr623 is predicted to hydrogen bond with the dimethylamine NH group of the sertindole analog. The predicted binding mode of this blocker is considerably different from sertindole, as is the crown-shaped hydrophobic volume, which is considerably more interrupted (Fig. 12B). This volume is occupied by the majority of the fluorophenyl group, part of the benzene group of the indole, and one methyl of the dimethylamine group. The propeller-shaped hydrophilic volume is occupied by the basic dimethylamine NH group.

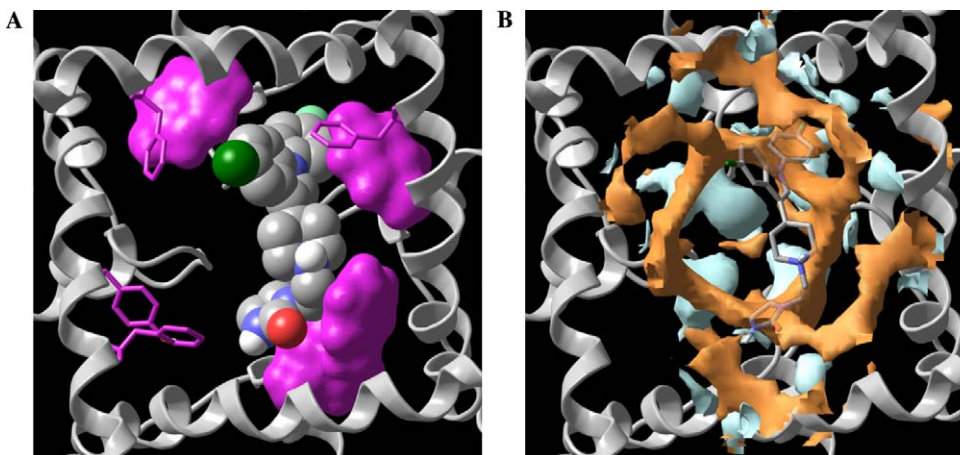


Figure 11. (A) Induced fit docking pose showing molecular surface contacts of the side chains of Tyr652 and Phe656 (magenta) with sertindole. (B) Overlap of sertindole with the hydrophobic (orange) and hydrophilic (cyan) iso-potential energy contours. Hydrogen atoms are not shown. The dark green atom in the foreground is Cl and the light green is F.

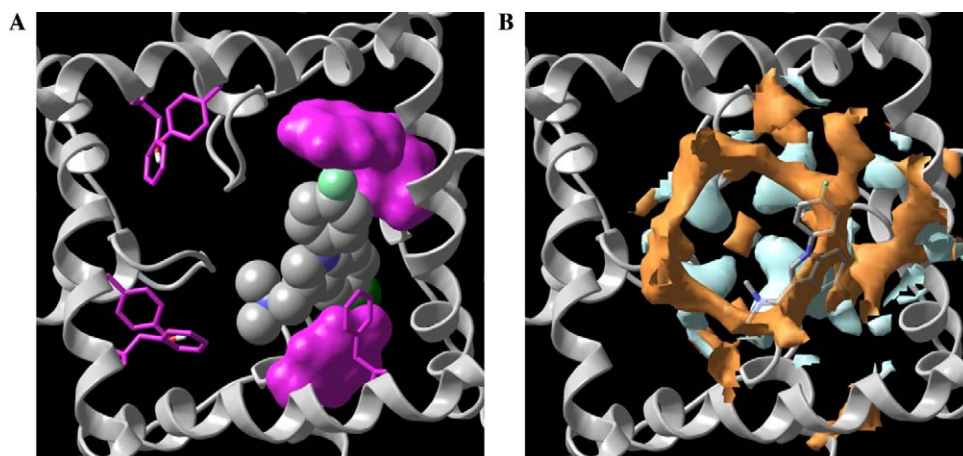


Figure 12. (A) Induced fit docking pose showing molecular surface contacts of the side chains of Tyr652 and Phe656 (magenta) with sertindole A5. (B) Overlap of sertindole A5 with the hydrophobic (orange) and hydrophilic (cyan) iso-potential energy contours. Hydrogen atoms are not shown. The light green atom in the foreground is F and the dark green is Cl.

3.10. Sertindole A1–A4

We compared the predicted binding interactions in four closely related carboxylate and methylcarboxyester analogs of sertindole. Replacement of fluoro by carboxylate (sertindole A1) results in a 25,000-fold loss in activity ($75\ \mu\text{M}$), whereas replacement by methylcarboxylate (sertindole A2) results in a 200-fold loss in activity ($579\ \text{nM}$). Replacement of fluoro by carboxylate methyl ester (sertindole A4) and methylcarboxylate methyl ester (sertindole A3) results in 12-fold ($36\ \text{nM}$) and 43-fold ($131\ \text{nM}$) losses in activity, respectively. Our docking results for sertindole and the four analogs (presented below) are highly consistent with these observations. All the high scoring sertindole poses predicted by the induced fit docking protocol can be clustered into four different conformations; the one shown in Figures 12A and 13A is clearly favored by GlideScore and Prime energy. The other three lower scoring poses (not shown) are similar to those found for the four analogs (Fig. 13B). The

imidazolidinone group of the top scoring pose for sertindole is directed toward the intracellular end of the pore and hydrogen bonded to Ser649 (Fig. 13A). The imidazolidinone group of all four sertindole analogs is directed toward the extracellular end of the pore near the selectivity filter and forms a hydrogen bond to the backbone carbonyl of Leu622. A remarkably good correlation ($R^2 = 0.95$) between XP GlideScore and experimental binding affinity (as estimated from the IC_{50} values) is observed for sertindole and analogs A1–A4 (Fig. 14). The Glide-XP lipophilic contact term for sertindole contributes to the favorable GlideScore for this $3\ \text{nM}$ blocker. The Glide-XP penalty for buried polar groups for sertindole A1 contributes to the unfavorable GlideScore for this $75\ \mu\text{M}$ blocker. Not surprisingly, the penalty for buried polar groups for sertindole A2 (which extends the carboxylate group $1.5\ \text{\AA}$ toward the intracellular end of the pore) is lower by about $1\ \text{kcal/mol}$. This penalty for the methyl ester analogs (A3 and A4) is also low. In addition, the Glide-XP van der Waals energy

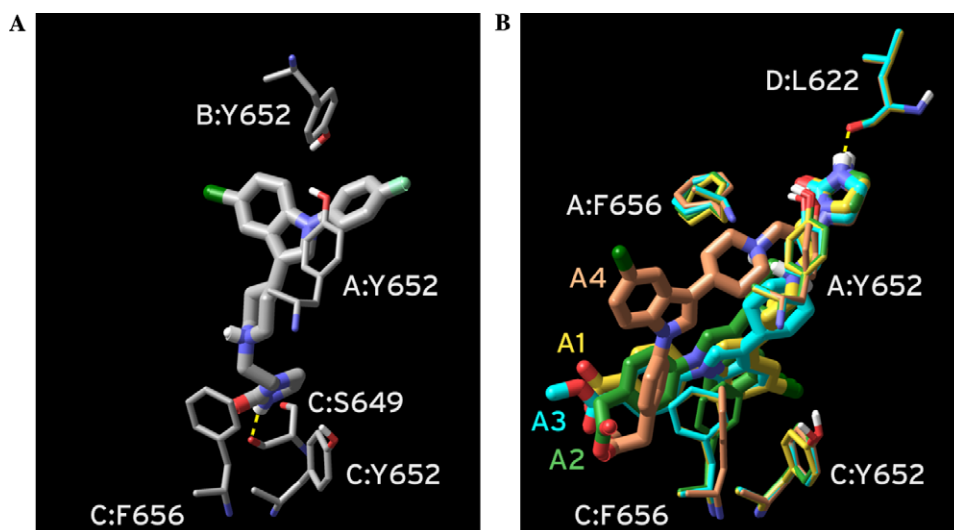


Figure 13. (A) Induced fit docking pose of sertindole and interacting Tyr652, Phe656, and Ser649 residues. (B) The same view showing induced fit docking poses of the sertindole analogs A1–A4. The intracellular region of HERG is on the bottom left and the extracellular on the top right.

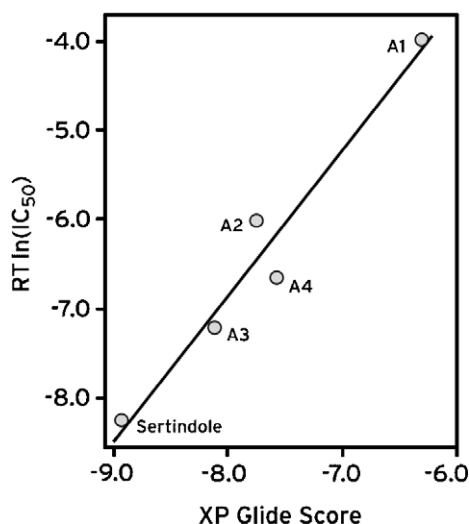


Figure 14. Plot of XP GlideScore versus an estimate of the free energy of binding, $RT \ln(IC_{50})$.

terms for the A3 and A4 analogs are more favorable than those of A1 and A2.

4. Discussion

Unlike other potassium channels, the ion conduction pathway of HERG is highly conducive to the formation of binding interactions with chemically diverse organic compounds containing aromatic, hydrophobic, and basic groups. The susceptibility of HERG to chemical blockade has been attributed to the unique, simultaneous presence of Tyr652 and Phe656 within the lumen of the pore domain,^{5,15–17} and the enhanced volume of the pore compared to KvX channels due to the absence of Pro at positions 655 and 657.⁴ The binding sensitivities of terfenadine, cisapride, and MK-499 to substitutions of Tyr652 and Phe656 with aromatic, aliphatic, polar, and charged residues were investigated by Fernandez et al.¹⁶ Tyr652Trp and Tyr652Phe mutations were found to retain activity, but not other residue types. Phe656 mutations to aliphatic or aromatic residues also retained activity. Furthermore, these authors identified a correlation between potency and hydrophobic surface area of the side chains of Phe656 substitutions.

Our docking and potential mapping studies provide additional insights about the basis for binding interactions and conformational requirements thereof. Multiple simultaneous aromatic π -stacking and/or hydrophobic interactions with various combinations of Tyr652 and Phe656 side chains were predicted in the most favorable docked poses of all blockers that we investigated. Our results suggest that two to four Tyr652, and one to two Phe656 side chains of the tetrameric pore domain are simultaneously involved in binding MK-499, cisapride, terfenadine, sertindole, ibutilide, and clofilium via hydrophobic and π -stacking interactions. This is highly consistent with the hydrophobic features predicted from 3D QSAR and pharmacophore

modeling studies. Large hydrophobic contributions can signify entropically driven binding. Under such conditions, losses of 46 \AA^2 of buried hydrophobic surface area can result in 10-fold losses in potency.⁴⁰

The requirement for an aromatic residue at sequence position 652, but not 656, has been attributed to π -cation interactions with highly prevalent basic blocker groups.^{8,9,12,16} This theory is based largely on the following indirect evidence: (1) activity requires an aromatic side chain (i.e., Tyr652) and often the simultaneous presence of a basic blocker group; (2) Tyr652 to Phe656 inter-side-chain distance is similar to the aromatic ring to basic group distance in some pharmacophore models.^{8,9} However, proximity between basic blocker groups and Tyr652 is not apparent in the docked poses of any blocker that we studied. Furthermore, IC_{50} differences observed for piperidyl versus des-piperidyl sertindole analogs are not consistent with the expected loss of 2.0–4.0 kcal/mol in binding energy contributed by a π -cation interaction.⁴¹ For example, the isopentyl sertindole analog (1.48 μM) is only 7-fold less active than its nearest piperidine-containing des-ethylcyclourea sertindole analog (204 nM),⁸ corresponding to less than 1 kcal/mol difference in free energy.⁴⁰ Given the critical role of Tyr652 established from site-directed mutagenesis studies, it seems likely that the loss of a π -cation interaction would result in a larger decrease in activity between sertindole and all of its des-piperidyl analogs. Our results suggest that the observed loss of binding sensitivity with mutation to non-aromatic side chains at position 652 is due to the loss of π -stacking interactions with aromatic rings present in nearly all blockers. Although we did not quantitatively assess the nature of the predicted aromatic ring interactions, it appears that at least one Tyr652 side chain participates in ring stacking interactions in all docked complexes. Other possible effects of non-aromatic Tyr652 mutations on binding sensitivity, including protein structural rearrangements, cannot be ruled out. Such rearrangements could result from disruptions in intra-monomer packing between the side chains of Tyr652 and Thr623 (packed within a larger cluster involving Ser624 and Val625 in our homology model) or disruptions in inter-monomer packing (Fig. 3). The possible role of C-type inactivation in conferring blockade sensitivity introduces further uncertainties in our model. However, ‘repositioning’ mutagenesis studies performed on HERG and EAG (a homolog that does not inactivate and lacks blockade sensitivity) do not support a direct cause-effect relationship between inactivation and blockade sensitivity.¹⁷ Rather, these studies suggest that inactivation and blockade sensitivity share common requirements for the spatial positions of Tyr652 and Phe656, which converge for WT HERG and EAG mutants in which Tyr or Phe are shifted down one sequence position.¹⁷ Whether the S6 conformation in KvAP correctly predicts the exact spatial positions of these residues in HERG cannot be determined at this time. However, our model is consistent with the high degree of exposure of Tyr 652 and Phe 656 within the blocker accessible region of the pore.

Our results, taken with those of mutagenesis studies, raise the possibility that mutation of Tyr652 and Phe656 can affect binding directly via loss of interactions, and indirectly via changes in protein structure. Our results suggest that polar groups, including the highly prevalent basic nitrogen, tend to localize within the propeller-shaped hydrophilic volume (associated with Ser624 and adjacent backbone atoms). As such, activity enhancement associated with the presence of a basic center is likely due to electrostatic interactions in this region, rather than π -cation interactions with Tyr652. Binding sensitivity of Ser624Ala mutation was demonstrated for MK-499,⁵ clofilium, and ibutilide,¹⁵ which is consistent with this hypothesis. Unfortunately, binding sensitivity to Ser624Ala mutation was not tested for terfenadine and cisapride.⁵ Our calculations likely underestimate the strength of electrostatic interactions due to neglect of the explicit contributions of the pore helix dipole moments known to converge in this region. We speculate that the overall electrostatic properties of the binding site, including the contribution of the trans-membrane field, elicit favorable interactions with cationic species, and unfavorable interactions with anionic species, except where specific favorable binding interactions can be formed, for example, sertindole A2.

Our docking results suggest that the tendency of HERG to bind small organic compounds is due, in part, to the high effective concentration of aromatic/hydrophobic side chains lining the ion conduction pathway. The specific configuration of such residues in the open channel creates opportunities for multiple simultaneous ring stacking and hydrophobic interactions that can be achieved in multiple binding conformations/orientations. Structure–activity relationships among the sertindole series suggest that electrostatic interactions with a basic blocker group can contribute an additional 10- to 100-fold enhancement in potency (7-fold for piperidyl vs. isopentyl sertindole and 130-fold for dimethylamine vs. isopentyl sertindole). The symmetric, redundant nature of the key binding residues, Tyr652, Phe656, and Ser624 (four copies each), is suggestive of a low information content ‘host-guest’ type binding site compared to that of an enzyme or receptor.

A canonical blocker topology consisting of a set of hydrophobic/aromatic groups arranged radially around a basic center is suggested from several published pharmacophore models. Our potential energy mapping and docking results are consistent with this overall topology. However, our results largely differ from published ligand-based models with respect to bound conformation and the specific nature of protein–ligand interactions. Our results suggest that blockers fold into ‘U-shaped’ and other conformations adapted to the cylindrical symmetry of the pore and its hydrophobic crown. Ligand-based models predict extended conformations that necessitate longitudinal binding parallel to the pore axis (inconsistent with our docked poses, except for MK-499). Our results further suggest that the basic nitrogen in blockers plays two critical roles in binding: (1) as a source of electrostatic interactions with Ser624 and nearby backbone atoms; (2) as a

branched center whose N-substituents bridge across the hollow interior of the hydrophobic crown and project aromatic/hydrophobic groups into the crown’s hydrophobic rim. This canonical motif is likely one of several possible topologies capable of satisfying the proposed binding constraints. MK-499, for example, exhibits a different topology and predicted binding geometry. In summary, the following ligand properties are suggested to play a key role in promoting HERG blockade:

1. Ability to form extensive ring stacking and/or hydrophobic interactions with Tyr652 and Phe656 side chains of multiple monomers, as reflected in the occupation of multiple sectors of a crown-shaped hydrophobic volume. Substituents arranged radially around a branched center (analogous to the hub and spokes of a wheel), for example, tri- or tetra-alkyl-substituted basic centers, represent a canonical binding motif,
2. ability of polar groups, and most notably a basic center, to interact with Ser624 and nearby polar backbone atoms, as reflected in the occupation of a propeller-shaped hydrophilic three-dimensional iso-potential energy contour,
3. ability to bind in multiple configurations under the constraints of requirements 1–2, suggesting that configurational entropy plays a key role in binding,
4. ability to form hydrogen bonds with polar side chains or backbone atoms, and
5. attraction of a basic center by the negative field present within the pore.

The mechanisms of disruption of potassium conductance via occupation of the conduction pathway are poorly understood. Possible mechanisms include physical occlusion, changes in cross-sectional area, shape, resistance, and disruption of critical transport-dependent electrostatic properties of the pathway. The conduction pathway is only partially occluded in many of our docked complexes, suggesting that blockade is not adequately described by physical occlusion. Brownian dynamics simulations of potassium conductance were performed by Chung et al. using simplified models of KcsA, in which the radius of the intracellular pore entrance was varied.⁴² Their results suggest that conductance increases nonlinearly as a function of intra-pore radius, an effect that is largely due to the increased cross-sectional area of the pore, and lowering of the energy barrier located approximately two-thirds of the distance from the intracellular opening to the selectivity filter. If this model is at all applicable to HERG, blocker-induced changes in conductance could result from reduction in the cross-sectional area or shape of the intracellular cavity and/or alteration of the delicate electrostatic balance between charged groups/dipole moments of the intracellular entrance and potassium ions within the selectivity filter. Graphical visualization of the pore-lining surfaces of the blocked complexes predicts large effects on pore geometry, iso-potential energy contours, and side-chain and local backbone conformation, consistent with this hypothesis.

5. Conclusions

Our docking results suggest that blockers bind to the intracellular potassium conduction cavity of HERG via a common mechanism involving extensive hydrophobic and ring stacking interactions with combinations of Tyr652 and Phe656 side chains from at least two monomers (typically three to four). However, the specific number, combination, and types of interactions, that is, hydrophobic versus ring stacking, formed with these side chains can vary. Additionally, blocker-specific polar interactions and hydrogen bonds (including those arising from a basic center) are also predicted. Blocker sensitive conformational differences in the pore domain are predicted. Such differences are mainly associated with side chain rotamers of Tyr652 and Phe656. Possible approaches to mitigation of HERG activity include increasing the polarity of hydrophobic groups interacting with Tyr652 and Phe656, introducing electron-withdrawing groups to disrupt ring stacking, destabilizing the active ligand conformation, and introducing shape non-complementarity (i.e., steric clashing). Additional work is needed to more fully understand the specific nature of the interactions suggested from our docking studies and the factors that influence their energetic contributions to binding affinity (including protein–ligand conformational strain and entropy).

References and notes

- Pearlstein, R.; Vaz, R.; Rampe, D. *J. Med. Chem.* **2003**, *46*, 2017.
- Tseng, G. N. *J. Mol. Cell Cardiol.* **2001**, *33*, 835.
- Sanguinetti, M. C.; Zou, A. *Heart Vessels* **1997**(Suppl. 12), 170.
- Keating, M. T.; Sanguinetti, M. C. *Cell* **2001**, *104*, 569.
- Mitcheson, J. S.; Chen, J.; Lin, M.; Culbertson, C.; Sanguinetti, M. C. *Proc. Natl. Acad. Sci. U.S.A.* **2000**, *97*, 12329.
- Kang, J.; Chen, X. L.; Wang, H.; Ji, J.; Cheng, H.; Incardona, J.; Reynolds, W.; Viviani, F.; Tabart, M.; Rampe, D. *Mol. Pharmacol.* **2005**, *67*, 827.
- Recanatini, M.; Poluzzi, E.; Masetti, M.; Cavalli, A.; De Ponti, F. *Med. Res. Rev.* **2005**, *25*, 133.
- Pearlstein, R. A.; Vaz, R. J.; Kang, J.; Chen, X. L.; Preobrazhenskaya, M.; Shchekotikhin, A. E.; Korolev, A. M.; Lysenkova, L. N.; Miroshnikova, O. V.; Hendrix, J.; Rampe, D. *Bioorg. Med. Chem. Lett.* **2003**, *13*, 1829.
- Cavalli, A.; Poluzzi, E.; De Ponti, F.; Recanatini, M. *J. Med. Chem.* **2002**, *45*, 3844.
- Ekins, S.; Crumb, W. J.; Sarazan, R. D.; Wikel, J. H.; Wrighton, S. A. *J. Pharmacol. Exp. Ther.* **2002**, *301*, 427.
- Roche, O.; Trube, G.; Zuegge, J.; Pflimlin, P.; Alanine, A.; Schneider, G. *Chembiochem* **2002**, *3*, 455.
- Bains, W.; Basman, A.; White, C. *Prog. Biophys. Mol. Biol.* **2004**, *86*, 205.
- Aronov, A. M.; Goldman, B. B. *Bioorg. Med. Chem.* **2004**, *12*, 2307.
- Zolotoy, A. B.; Plouvier, B. P.; Beatch, G. B.; Hayes, E. S.; Wall, R. A.; Walker, M. *J. Curr. Med. Chem. Cardiovasc. Hematol. Agents* **2003**, *1*, 225.
- Perry, M.; de Groot, M. J.; Helliwell, R.; Leishman, D.; Tristani-Firouzi, M.; Sanguinetti, M. C.; Mitcheson, J. *Mol. Pharmacol.* **2004**, *66*, 240.
- Fernandez, D.; Ghanta, A.; Kauffman, G. W.; Sanguinetti, M. C. *J. Biol. Chem.* **2004**, *279*, 10120.
- Chen, J.; Seebom, G.; Sanguinetti, M. C. *Proc. Natl. Acad. Sci. U.S.A.* **2002**, *99*, 12461.
- Torres, A. M.; Bansal, P. S.; Sunde, M.; Clarke, C. E.; Bursill, J. A.; Smith, D. J.; Bauskin, A.; Breit, S. N.; Campbell, T. J.; Alewood, P. F.; Kuchel, P. W.; Vandenberg, J. I. *J. Biol. Chem.* **2003**, *278*, 42136.
- Liu, J.; Zhang, M.; Jiang, M.; Tseng, G. N. *J. Gen. Physiol.* **2002**, *120*, 723.
- Andrec, M.; Harano, Y.; Jacobson, M. P.; Friesner, R. A.; Levy, R. M. *J. Struct. Funct. Genomics* **2002**, *2*, 103.
- Jacobson, M. P.; Friesner, R. A.; Xiang, Z. X.; Honig, B. *J. Mol. Biol.* **2002**, *320*, 597.
- Jacobson, M. P.; Pincus, D. L.; Rapp, C. S.; Day, T. J.; Honig, B.; Shaw, D. E.; Friesner, R. A. *Proteins* **2004**, *55*, 351.
- Li, X.; Jacobson, M. P.; Friesner, R. A. *Proteins* **2004**, *55*, 368.
- Jiang, Y.; Lee, A.; Chen, J.; Cadene, M.; Chait, B. T.; MacKinnon, R. *Nature* **2002**, *417*, 523.
- Desta, Z.; Soukhova, N.; Moroch, A. M.; Flockhart, D. A. *J. Pharmacol. Exp. Ther.* **2001**, *298*, 508.
- Halgren, T. A.; Murphy, R. B.; Friesner, R. A.; Beard, H. S.; Frye, L. L.; Pollard, W. T.; Banks, J. L. *J. Med. Chem.* **2004**, *47*, 1750.
- Friesner, R. A.; Banks, J. L.; Murphy, R. B.; Halgren, T. A.; Klicic, J. J.; Mainz, D. T.; Repasky, M. P.; Knoll, E. H.; Shelley, M.; Perry, J. K.; Shaw, D. E.; Francis, P.; Shenkin, P. S. *J. Med. Chem.* **2004**, *47*, 1739.
- Sherman, W.; Day, T.; Jacobson, M. P.; Friesner, R. A.; Farid, R. *J. Med. Chem.* (in press).
- Witchel, H. J.; Dempsey, C. E.; Sessions, R. B.; Perry, M.; Milnes, J. T.; Hancox, J. C.; Mitcheson, J. S. *Mol. Pharmacol.* **2004**, *66*, 1201.
- Gonzalez, T.; Arias, C.; Caballero, R.; Moreno, I.; Delpon, E.; Tamargo, J.; Valenzuela, C. *Br. J. Pharmacol.* **2002**, *137*, 1269.
- Waldegger, S.; Niemeyer, G.; Morike, K.; Wagner, C. A.; Suessbrich, H.; Busch, A. E.; Lang, F.; Eichelbaum, M. *Cell Physiol. Biochem.* **1999**, *9*, 81.
- Mao, L.; Wang, Y.; Liu, Y.; Hu, X. *J. Mol. Biol.* **2004**, *336*, 787.
- Sinnokrot, M. O.; Sherrill, C. D. *J. Phys. Chem. A* **2004**, *108*, 10200.
- Sinnokrot, M. O.; Valeev, E. F.; Sherrill, C. D. *J. Am. Chem. Soc.* **2002**, *124*, 10887.
- Sinnokrot, M. O.; Sherrill, C. D. *J. Am. Chem. Soc.* **2004**, *126*, 7690.
- Obst, U.; Betschmann, P.; Lerner, C.; Seiler, P.; Diederich, F. *Helv. Chim. Acta* **2000**, *83*, 855.
- Turk, J. A.; Smithrud, D. B. *J. Org. Chem.* **2001**, *66*, 8328–8335.
- Zhang, S.; Barr, B. K.; Wilson, D. B. *Eur. J. Biochem.* **2000**, *267*, 244.
- Kumar, M.; Kannan, K. K.; Hosur, M. V.; Bhavesh, N. S.; Chatterjee, A.; Mittal, R.; Hosur, R. V. *Biochem. Biophys. Res. Commun.* **2002**, *294*, 395.
- Kuntz, I. D.; Chen, K.; Sharp, K. A.; Kollman, P. A. *Proc. Natl. Acad. Sci. U.S.A.* **1999**, *96*, 9997.
- Zacharias, N.; Dougherty, D. A. *Trends Pharm. Sci.* **2002**, *23*, 281.
- Chung, S. H.; Allen, T. W.; Kuyucak, S. *Biophys. J.* **2002**, *82*, 628.